Doping-Dependent Negative Differential Resistance in Hybrid Organic/Inorganic Si–Porphyrin–Si Junctions

Filipe J. Ribeiro,[†,§] Wenchang Lu,[†,‡] and Jerzy Bernholc[†,‡,*]

[†]Center for High Performance Simulation and Department of Physics, North Carolina State University, Raleigh, North Carolina 27695-7518, and [‡]Computer Science and Mathematics Division, Oak Ridge National Laboratory, Oak Ridge, Tennessee 37831-6367. [§]Present address: Department of Physics, University of California at Berkeley, Berkeley, CA 94720.

ARTICLE

ABSTRACT Quantum transport properties of porphyrin-bridged p–n junctions with Si leads are investigated by *ab initio* calculations. It is shown that this system exhibits strong negative differential resistance (NDR) peaks, whose magnitude and position can be controlled by the doping levels of the leads and by changing the central transition metal atom of the porphyrin. These results are explained by bias-induced on–off switching of resonant tunneling channels associated with specific molecular orbitals. The predicted behavior is general and should be observable for other organic molecules bridging doped semiconducting leads.

KEYWORDS: porphyrin · quantum transport · negative differential resistance · silicon · doping

In 1974, Aviram and Ratner[1] proposed using organic molecules as alternatives to conventional methods of building electronic devices. Since then, a significant amount of research has been carried out to explore the feasibility and intrinsic properties of such devices.[2,3] Examples of possible applications include single-electron transistors consisting of a single organic molecule bridging two gold electrodes[4] and memory devices based on self-assembled monolayers (SAMs) of organic molecules on surfaces. The real-world reliability of such molecular memory devices has already been demonstrated,[5] and more recently, a strong dependence of the redox voltages and rates on doping of the semiconductor leads and ambient light exposure[6] has been described. Additionally, the negative differential effect (NDR), present in conventional resonant tunneling diodes, and which can be explored to build fast switches and high-frequency oscillators,[7] has also been observed in measurements of current–voltage characteristics of organic molecules on gold[8] and silicon[9,10] surfaces. In the former case, a current peak-to-valley ratio (PVR) of 1000:1 was reached, due to voltage-induced reduction of a nitroamine center. Theoretical investigations with either *ab initio* or empirical methods have been carried out for molecules on both metallic[11–16] and semicondutor surfaces.[17–19]

In this paper, we demonstrate, from a theoretical standpoint, that NDR characteristics of a molecule sandwiched between semiconductor leads can be dramatically altered and tuned by doping of the leads and/or atomic substitution in the bridging molecule. A technologically important Si–porphyrin–Si system is used as a paradigmatic example, with different atoms in the center of the porphyrin ring. In each case, sharp NDR peaks are obtained, whose positions and strengths change with the central atoms. Furthermore, the kind, number, and PVR of the NDR peaks are tunable by doping the Si leads with extra carriers. Similar results are expected for a wide class of small and medium-size molecules bridging doped semiconducting leads.

RESULTS AND DISCUSSION

We consider three different porphyrin (Por) molecules, H_2–Por, Zn–Por, and Ni–Por. Figure 1 shows the atomic structures of two systems consisting of either a H_2–Por or a Zn–Por molecule bridging two Si surfaces. The center of the H_2–Por is composed of four N atoms, two of which are bonded to H atoms, while the center of Zn–Por is composed of four N atoms bonded to a single Zn atom. We also consider Ni–Por, where the Zn in Zn–Por is replaced by a Ni atom. The porphyrins in this work are tethered on both sides by two benzyl alcohol groups and connect to Si(100) surfaces through O–Si chemical bonds—similarly to the ones studied in refs 5 and 20. The Si(100) surfaces can be

*Address correspondence to bernholc@ncsu.edu.

Received for review April 29, 2008 and accepted June 23, 2008.

Published online July 11, 2008.
10.1021/nn800252b CCC: $40.75

© 2008 American Chemical Society

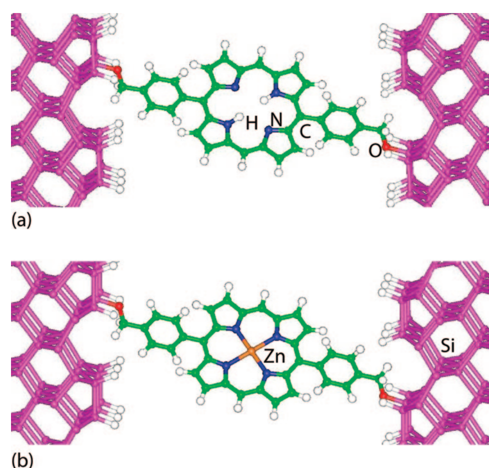

Figure 1. Two model structures of porphyrins (Por) tethered by benzyl alcohols: (a) H_2−Por and (b) Zn−Por molecules, chemically bonded to two H-passivated Si(100) surfaces. The structure of the Ni−Por bridged device is similar to (b). Atom colors are H: white, C: green, O: red, N: blue, Si: magenta, Zn: brown. Note that all systems have inversion symmetry.

described as a monohydride 2 × 1 dimer row reconstruction.[21]

The effects of doping were represented by applying shifts to the chemical potentials of the leads. A positive chemical potential shift increases the number of electrons in the conduction band, while a negative shift adds holes to the valence band. The chemical potentials for different doping levels are obtained by solving numerically for μ using the equation

$$N_e = \int_{-\infty}^{\infty} n_e(E) f((E-\mu)/k_BT) dE$$

where N_e is the total number of electrons, $n_e(E)$ is the electron density of states, $f(x)$ is the Fermi−Dirac distribution, and T is the room temperature. Three doping levels are considered: undoped intrinsic leads; doped leads with 10^{16} carriers per cm^3 (shift of 0.10 eV); and doped leads with 10^{19} carriers per cm^3 (shift of 0.27 eV), with the left lead n-doped and the right lead p-doped.[22]

Figure 2 shows the forward-bias current as a function of forward-bias voltage for the three systems studied. In the undoped case, the reverse-bias current is the same as the forward-bias current due to inversion symmetry. As will be shown below, the doping-dependent current peaks obtained under forward-bias emerge when the electron-rich conduction band minimum (CBM) of the n-doped lead is aligned with an unoccupied molecular orbital or when the hole-rich valence band maximum (VBM) of the p-doped lead is aligned with an occupied molecular orbital. Under reverse-bias conditions, when the electron-poor CBM of the p-doped lead (or the hole-poor VBM of the n-doped lead) is aligned with a LUMO (or a HOMO), there is no current increase because no extra carriers are available for resonant tunneling. At a very large bias, the CBM of the p-doped lead (or the VBM of the

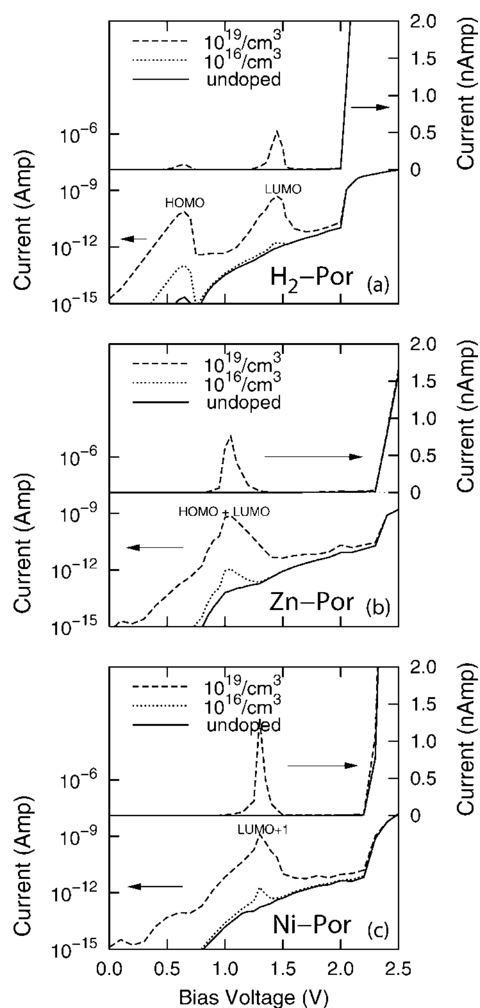

Figure 2. Current *versus* voltage plots in log (bottom plots, left axis) and linear (top plots, right axis) scales for (a) H_2−Por, (b) Zn−Por, and (c) Ni−Por, for various Si doping levels. Doping levels are 0 (solid), $10^{16}/cm^3$ (dotted line), and $10^{19}/cm^3$ (dashed line). See text.

n-doped lead) is aligned with a HOMO (or LUMO), then the current will increase monotonically, which is similar to the undoped case except for the bias shift as discussed below. Therefore, the reverse-bias currents are essentially independent of doping levels and similar to the undoped forward-bias current; hence, they are not shown.

For all the doped and undoped systems, we refer to the effective zero bias voltage as the voltage at which the left and right band gaps of the Si leads are aligned. In actual devices, the chemical potentials of the leads are aligned at zero bias, which results in a doping-dependent displacement of the band gaps equal to the difference between the left and right chemical potentials. This shifts the peaks in the current *versus* voltage graphs by the amount of doping-induced displacement. In order to simplify the discussion of the physical origins of the results, the doping-dependent currents are plotted relative to the effective zero bias, but they can easily be corrected by adding the shifts given above. These shifts are analogous to the observed n *ver-*

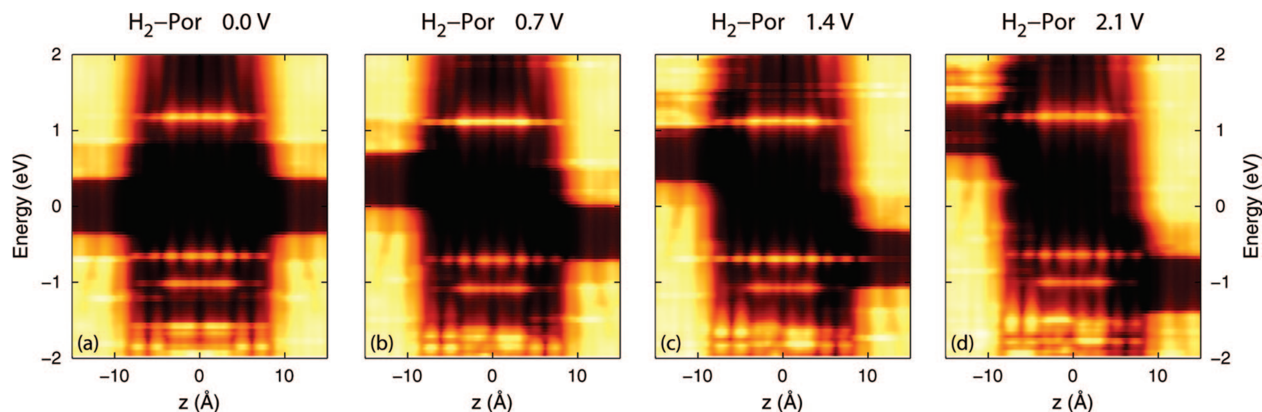

Figure 3. Spatially resolved energy density of states for H_2-Por at biases of (a) 0.0 V, (b) 0.7 V, (c) 1.4 V, and (d) 2.1 V. The energy 0 is set to the average of the left and right chemical potentials. Light (dark) colors correspond to high (low) electron densities.

sus p doping asymmetry in doping-dependent redox rates reported in ref 6.

The alignment of the energy levels of H_2−Por and the Si leads for different biases is apparent in the spatially resolved density of states plots in Figure 3. In the undoped configuration of H_2−Por (solid line in Figure 2a), the current turns on at the bias of 0.8 V, which corresponds to the value of the density functional theory energy gap in the Si leads.[23,24] At this voltage, electrons with energies close to the VBM of the left lead start to tunnel to the unoccupied states at the CBM of the right lead. For higher voltages, more electrons are able to tunnel and the current increases accordingly. At 2.1 V, the current increases by 2 to 3 orders of magnitude (see Figure 2a) because, at this voltage, the energy of the HOMO of H_2−Por is aligned with the right CBM, which results in the opening of a resonant tunneling channel between the two leads.

Figure 2a also shows how the current behaves for doped systems (dashed and dotted lines) when the left lead is n-doped and the right lead is p-doped. At biases below 2 V, the current shows very strong peaks relative to the current of the undoped system, while above 2 V, the current is independent of doping. All the current peaks found in our calculations are associated with resonant transmission through molecular orbitals (*e.g.*, HOMO, LUMO, LUMO+1, *etc.*) from pockets of extra carriers—either electrons or holes. When the bias voltage is raised so that the energy of the resonant orbital falls into the gap of one of the leads, the channel closes, the current drops, and NDR occurs. However, the only orbitals that behave as resonant channels are those for which the electron density extends throughout the entire molecule and that hybridize significantly with the Si states.

The first current peak for the doped systems in Figure 2a at 0.7 V (and a PVR of 200:1 for the strong doping case) is due to the alignment of the energy of the HOMO of H_2−Por with the energy of the holes of the VB of the p-doped right lead (see Figure 3b). Above this voltage, the energy of the HOMO falls into the gap of the right lead and the current drops. On the other hand, the second peak in Figure 2a at 1.4 V and PVR of 80:1 results from the energy alignment of the extra electrons in the CB of the n-doped left lead with the porphyrin LUMO (see Figure 3c). Once the applied voltage drives the porphyrin LUMO energy into the gap of the left lead, this channel is closed and the current drops with bias. The heights of the peaks are clearly proportional to the number of extra holes (electrons) present on each lead. As the doping level is increased from $10^{16}/cm^3$ (dotted lines) to $10^{19}/cm^3$ (dashed lines), the peak heights increase by 3 orders of magnitude.

At voltages above 2.0 V, the dominant current is due to resonant tunneling of left lead VB electrons through the porphyrin HOMO—as seen above for the undoped system—and the effects of doping are negligible.

Figure 2b,c shows the current as a function of bias for the Zn−Por and Ni−Por systems, and Figure 4 shows the spatially resolved densities of states at representative bias voltages. The molecular orbitals that work as resonant channels in Zn−Por are the HOMO and the LUMO. In Ni−Por, on the other hand, the HOMO, the degenerate HOMO-1 and HOMO-2, and the LUMO are localized around the Ni atom and are

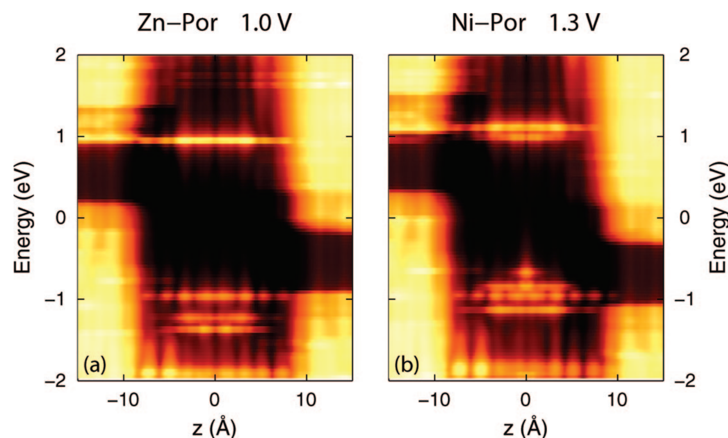

Figure 4. Spatially resolved density of states for (a) Zn−Por at 1.0 V and (b) Ni−Por at 1.3 V. The energy 0 is set to the average of the left and right chemical potentials. Light (dark) colors correspond to high (low) electron densities.

not strongly coupled with the Si states. Figure 4b shows the limited spacial extent of these orbitals. The orbital associated with resonant tunneling is the LUMO+1 (and to a lesser extent the HOMO-3), which spatially bridge the separation between the two leads.

As was the case for H_2−Por, in the undoped Zn−Por and Ni−Por systems, the current turns on around 0.8 V and increases with voltage, due to direct tunneling of electrons from the left VB to the right CB. At bias voltages of 2.3 V for Zn−Por and 2.2 V for Ni−Por, the HOMO and LUMO of Zn−Por and the LUMO+1 of Ni−Por establish resonant channels between the left and right leads, increasing the current by 2 to 3 orders of magnitude (see Figure 2b,c).

Turning to the doping-dependent current peaks, Figure 2b shows a peak at 1.0 V, with a PVR of 140:1, for the heavily doped Zn−Por system. Coincidentally, at this voltage, both the HOMO and the LUMO are aligned with the right VB and the left CB, respectively (see Figure 4a).[25] Therefore, both orbitals work as resonant channels between the leads until the bias increases and their energies fall into the Si gaps.

Figure 2c shows the behavior of the current as a function of bias voltage for the Ni−Por system. For the doped systems, the current peaks around 1.3 V with a PVR of 230:1 for the strongly doped configuration. Figure 4b shows how the Ni−Por LUMO+1, which is associated with this peak, aligns with the left CB minimum and establishes a resonant channel with the right VB. Among the systems considered here, the Ni−Por has the largest PVR. Further enhancement of the PVR may be obtained by additional doping, which could be tuned to specific applications.

The above results also explain the experimentally observed variation in redox voltages and kinetics for Zn(II) trimesitylporphyrin (Por-BZOH)[6] adsorbed on doped Si. Por-BZOH can exist in neutral and single and double oxidation states. Its redox voltage was shown to be strongly dependent on doping levels for n-Si but not for p-Si. The cationic-accessible state is the HOMO, which is located below the valence band maximum, just as in our calculations for H_2−Por. In experiments, the p-doped Si lead readily accepts electrons from the molecule because of the presence of holes in the valence band. However, in the n-Si case, holes are not available in the valence band to recombine with electrons from the molecule and must be generated either thermally or optically to allow the oxidation to proceed. These experimental results are completely consistent with ours. The first current peak in the H_2−Por system at 0.7 V (Figure 2b) corresponds to electrons being transferred from the molecule, as in oxidation, to the right p-doped lead, while they are being replenished by the left n-Si lead (reduction). The level diagram for this process, which includes the density of states of the leads, is shown in Figure 3b. However, if the leads were reversed, the molecule would not be able to oxidize since there would be no holes in the right n-Si lead, analogously to the limited oxidation of PorBzOH on n-Si substrates in ref 6.

SUMMARY AND CONCLUSIONS

In summary, this paper investigated a novel, porphyrin-bridged p−n junction through *ab initio* electronic transport calculations. It predicts that this and similar systems exhibit strong NDR characteristics, which can be tuned by varying the doping levels of the leads and/or by modifying the atomic structure of the molecule. For undoped systems, the current turns on for bias voltages above the energy gap of the leads and increases monotonically with voltage, as electrons directly tunnel from the VB of the left lead to the CB of the right lead. At high voltages, direct tunneling between the VB maximum of the left lead and the CB minimum of the right lead increases the current by 2 to 3 orders of magnitude. For doped systems, carrier-density-dependent current peaks are observed at intermediate bias voltages. These peaks arise as a result of resonant tunneling through molecular orbitals that bridge pockets of extra holes or electrons on one electrode and the VB or CB on the other electrode. NDR results when the energy of the MO forming the resonant channel is driven into the gap of one of the Si leads. The shape and position of these current peaks can be tuned by changing the atoms in the center of the porphyrin (H_2−, Zn−, or Ni−). The strongest PVR found was for Ni−Por.

One should note that the behavior exhibited by these three systems should be very general. Any molecule with extended orbitals with energies close to the CBM and/or VBM of a semiconducting lead should exhibit current peaks and NDR for the appropriate voltages and doping levels. Additional control of the positions of current peaks and NDR could also be achieved by using a third lead or a substrate to supply gating voltage.

METHODOLOGY AND CALCULATIONS

In the transport calculations, a real-space implementation of the nonequilibrium Green's functions (NEGF) method[26,27] is used to compute the charge density and potential self-consistently. Our code is suitable to study very large systems, up to several thousand atoms.[15,18] The system is partitioned into three parts, the two Si leads and the scattering region, which includes the molecule and a few Si buffer layers on both sides. Both the leads and the scattering region are treated using density functional theory (DFT)[28,29] within the generalized gradient approximation (GGA)[30] to the exchange and correlation functional. The interactions of

the core electrons and nuclei with the valence electrons are described by ultrasoft pseudopotentials.[31]

The first step is to determine the optimized localized basis set by using the real-space multigrid code. The localized orbitals centered at atoms are variationally optimized.[32,33] Five orbitals per hydrogen, carbon, nitrogen, oxygen, and silicon atoms, and nine orbitals per nickel and zinc atoms are found to be accurate enough to converge the total energy within 10 meV. None of the calculations are spin-polarized since it has been shown[34] that the Ni−Por and Zn−Por molecules are closed shell.

The atomic positions of the Si−Por−Si systems are relaxed in several stages due to the large number of degrees of freedom involved. First, the isolated porphyrin molecules are fully relaxed. Second, the bond between a Si surface atom and an OCH_3 group is optimized since the porphyrin molecules are attached to the Si surface through an alcohol group. Next, the full molecule is attached, and further relaxation steps are performed. Finally, the molecule is matched to the other Si lead through an identical Si−O bond, and a last relaxation step is performed. The resulting tilt angle between the porphyrin axis and the Si surfaces is 77°, with the phenyl ring planes forming a 60° angle with the porphyrin plane. The final forces were converged to better than 0.004 Ha/Bohr. The final binding energy, calculated as the total energy difference between the isolated H-passivated Si surfaces plus an isolated porphyrin molecule and the Si−Por−Si junction plus two isolated H_2 molecules, is 0.8 eV.

The Si lead calculations use unit cells with 8 layers of Si atoms with 12 atoms per layer, corresponding to a 4 × 3 surface unit cell. In terms of *k*-point sampling, a Γ-point calculation with a 4 × 3 supercell corresponds to a 12 *k*-point calculation in a 1 × 1 unit cell. In our case of semiconductor leads, the *I*−*V* characteristics are mainly band-gap-related, and the DFT band gap is well reproduced with this sampling. The unit cell for the scattering region consists of 12 layers of Si for each of the leads plus the porphyrin molecule.

Once the localized basis set is determined, the second step is to calculate the charge density matrix within the NEGF method. In the optimized basis set $\varphi(r)$, the charge density matrix can be written as

$$D_{\mu\nu} = \frac{1}{\pi}\int_{-\infty}^{\infty} [[G_C^+(E)\Gamma_L(E)G_C^-(E)]_{\mu\nu} f(E-\mu_L) + [G_C^+(E)\Gamma_R(E)G_C^-(E)]_{\mu\nu} f(E-\mu_R)]dE$$

where $f(E)$ is the Fermi−Dirac occupation and μ_L and μ_R are the chemical potentials of the left and right leads, respectively. $G_C^{\pm}$ are the retarded and advanced Green's functions of the scattering region. A complex energy contour integration[27] is used to obtain the charge density matrix efficiently.

The charge density in the scattering region is

$$\rho(\mathbf{r}) = \sum_{\mu,\nu} \varphi_\mu(\mathbf{r}) D_{\mu\nu} \varphi_\nu(\mathbf{r})$$

where the $\varphi_{\mu,\nu}(\mathbf{r})$ are the optimized localized orbitals. The Hartree potentials at the different bias voltages are obtained by solving the Poisson's equation with boundary conditions adjusted to match the left and right chemical potential shifts. For each bias voltage, a self-consistency cycle is performed to get the converged potential and charge density in the scattering region. It has been established that self-consistency is fundamental to the correct identification of current peaks and NDR.[18]

The final step is to calculate the current under bias after the potential and charge density are self-consistently determined. The current *I* as a function of bias voltage *V* is obtained by integrating the transmission coefficient $T(E, V)$:

$$I(V) = \int_{-\infty}^{\infty} T(E, V)[f(E-\mu_L) - f(E-\mu_R)]dE$$

The transmission coefficient $T(E, V)$ is calculated using

$$T(E, V) = \frac{2e^2}{h}\mathrm{Tr}[\Gamma_L(E)G_C^+(E)\Gamma_R(E)G_C^-(E)]$$

The bias voltage *V* does not appear explicitly on the right-hand side of the above equation. However, the Green's functions are calculated using the self-consistently determined potentials which depend on the bias voltage *V*. The coupling between the semi-infinite leads and the scattering region is described by $\Gamma_{L,R} = i[\Sigma_{L,R}^+ - \Sigma_{L,R}^-]$, where $\Sigma_{L,R}^{\pm}$ are the self-energies.

Additionally, the Green's function of the whole system gives the spectral function $A = i[G^- - G^+]$, from which the localized density of states can be calculated:

$$\rho(r, E) = \frac{1}{2\pi}\sum_{i,j} \varphi_i^*(r) A_{ij}(E) \varphi_j(r)$$

where φ_i are the localized orbitals.

Acknowledgment. This work was supported by NSF, ONR, and DOE. Computational resources were provided by the DoD Challenge Program and ORNL.

Note added after ASAP publication: Due to a production error, the caption of Figure 4 was also used as the caption for Figure 3 in the version published July 11, 2008. The corrected version was published ASAP August 5, 2008.

REFERENCES AND NOTES

1. Aviram, A.; Ratner, M. A. Molecular Rectifiers. *Chem. Phys. Lett.* **1974**, *29*, 277–283.
2. Joachim, C.; Ratner, M. A. Molecular Electronics: Some Views on Transport Junctions and Beyond, *Proc. Natl. Acad. Sci. U.S.A.* **2005**, *102*, 8801–8808.
3. Nitzan, A.; Ratner, M. Electron Transport in Molecular Wire Junctions. *Science* **2003**, *300*, 1384–1389.
4. Kubatkin, S.; Danilov, A.; Hjort, M.; Cornil, J.; Brédas, J.-L.; Stuhr-Hansen, N.; Hedegoard, P.; Bjornholm, T. Single-Electron Transistor of a Single Organic Molecule With Access to Several Redox States. *Nature* **2003**, *425*, 698–701.
5. Liu, Z.; Yasseri, A. A.; Lindsey, J. S.; Bocian, D. F. Molecular Memories That Survive Silicon Device Processing and Real-World Operation. *Science* **2003**, *302*, 1543–1545.
6. Gowda, S.; Mathur, G.; Misra, V. Valence Band Tunneling Model for Charge Transfer of Redox-Active Molecules Attached to n- and p-Silicon Substrates. *Appl. Phys. Lett.* **2007**, *90*, 142113.
7. Brown, E.; Söderström, J.; Parker, C.; Mahoney, L.; Molvar, K.; McGill, T. Oscillations up to 712 GHz in InAs/AlSb Resonant-Tunneling Diodes. *Appl. Phys. Lett.* **1991**, *58*, 2291–2293.
8. Chen, J.; Reed, M. A.; Rawlett, A. M.; Tour, J. M. Large On-Off Ratios and Negative Differential Resistance in a Molecular Electronic Device. *Science* **1999**, *286*, 1550–1552.
9. Guisinger, N. P.; Greene, M. E.; Basu, R.; Baluch, A. S.; Hersam, M. C. Room Temperature Negative Differential Resistance through Individual Organic Molecules on Silicon Surfaces. *Nano Lett.* **2004**, *4*, 55–59.
10. Guisinger, N. P.; Basu, R.; Baluch, A. S.; Hersam, M. C. Observed Suppression of Room Temperature Negative Differential Resistance in Organic Monolayers on Si(100). *Nanotechnology* **2004**, *15*, S452–S458.
11. Di Ventra, M.; Pantelides, S. T.; Lang, N. D. First-Principles Calculation of Transport Properties of a Molecular Device. *Phys. Rev. Lett.* **2000**, *84*, 979–982.
12. Di Ventra, M.; Kim, S. G.; Pantelides, S. T.; Lang, N. D. Temperature Effects on the Transport Properties of Molecules. *Phys. Rev. Lett.* **2001**, *86*, 288–291.
13. Xue, Y.; Datta, S.; Ratner, M. A. Charge Transfer and Band Lineup in Molecular Electronic Devices: A Chemical and Numerical Interpretation. *J. Chem. Phys.* **2001**, *115*, 4292–4299.

ARTICLE

14. Ke, S.; Baranger, H.; Yang, W. Electron Transport Through Molecules: Self-Consistent and Non-Self-Consistent Approaches. *Phys. Rev. B* **2004**, *70*, 85410.
15. Wang, S.; Lu, W.; Zhao, Q.; Bernholc, J. Resonant Coupling and Negative Differential Resistance in Metal/Ferrocenyl Alkanethiolate/STM Structures. *Phys. Rev. B* **2006**, *74*, 195430.
16. Delaney, P.; Greer, J. C. Correlated Electron Transport in Molecular Electronics. *Phys. Rev. Lett.* **2004**, *93*, 036805.
17. Rakshit, T.; Liang, G. C.; Ghosh, A. W.; Datta, S. Silicon-Based Molecular Electronics. *Nano Lett.* **2004**, *4*, 1803–1807.
18. Lu, W.; Meunier, V.; Bernholc, J. Nonequilibrium Quantum Transport Properties of Organic Molecules on Silicon. *Phys. Rev. Lett.* **2005**, *95*, 206805.
19. Rakshit, T.; Liang, G.; Ghosh, A.; Hersam, M.; Datta, S. Molecules on Silicon: Self-Consistent First-Principles Theory and Calibration to Experiments. *Phys. Rev. B* **2005**, *72*, 125305.
20. Li, Q.; Mathur, G.; Gowda, S.; Surthi, S.; Zhao, Q.; Yu, L.; Lindsey, J. S.; Bocian, D. F.; Misra, V. Multibit Memory Using Self-Assembly of Mixed Ferrocene/Porphyrin Monolayers on Silicon. *Adv. Mater.* **2004**, *16*, 133–137.
21. Boland, J. Structure of the H-Saturated Si(100) Surface. *Phys. Rev. Lett.* **1990**, *65*, 3325–3328.
22. The employed doping densities are much smaller than the valence electron density in Si, $\sim 2 \times 10^{23}/cm^3$. They were thus not taken into account in the self-consistent DFT calculations.
23. DFT calculations underestimate semiconductor HOMO−LUMO gaps. As a consequence, the specific voltages at which the various currents are turned on or peak are also underestimated.
24. Hybertsen, M. S.; Louie, S. G. Electron Correlation in Semiconductors and Insulators: Band Gaps and Quasiparticle Energies. *Phys. Rev. B* **1986**, *34*, 5390–5413.
25. This simultaneous alignment of levels could be an artifact of DFT.
26. Larade, B.; Taylor, J.; Mehrez, H.; Guo, H. Conductance, $I-V$ Curves, and Negative Differential Resistance of Carbon Atomic Wires. *Phys. Rev. B* **2001**, *64*, 075420.
27. Brandbyge, M.; Mozos, J. L.; Ordejon, P.; Taylor, J.; Stokbro, K. Density-Functional Method for Nonequilibrium Electron Transport. *Phys. Rev. B* **2002**, *65*, 165401.
28. Hohenberg, P.; Kohn, W. Inhomogeneous Electron Gas. *Phys. Rev.* **1964**, *136*, B864–B871.
29. Kohn, W.; Sham, L. J. Self-Consistent Equations Including Exchange and Correlation Effects. *Phys. Rev. A* **1965**, *140*, A1133–A1138.
30. Perdew, J. P.; Burke, K.; Ernzerhof, M. Generalized Gradient Approximation Made Simple. *Phys. Rev. Lett.* **1996**, *77*, 3865–3868.
31. Vanderbilt, D. Soft Self-Consistent Pseudopotentials in a Generalized Eigenvalue Formalism. *Phys. Rev. B* **1990**, *41*, 7892–7895.
32. Fattebert, J.-L.; Bernholc, J. Towards Grid-Based O(N) Density-Functional Theory Methods: Optimized Nonorthogonal Orbitals and Multigrid Acceleration. *Phys. Rev. B* **2000**, *62*, 1713–1722.
33. Buongiorno Nardelli, M.; Fattebert, J.-L.; Bernholc, J. O(N) Real-Space Method for *Ab Initio* Quantum Transport Calculations: Application to Carbon Nanotube Metal Contacts. *Phys. Rev. B* **2001**, *64*, 245423.
34. Liao, M.-S.; Scheiner, S. Electronic Structure and Bonding in Metal Porphyrins, Metal = Fe, Co, Ni, Cu, Zn. *J. Chem. Phys.* **2002**, *117*, 205–219.